# A multi-isotope model for simulating soil organic carbon cycling on an eroding landscape (WATEM_C v1.0)

Zhengang Wang[1,2], Kristof Van Oost[2]

[1] Guangdong Provincial Key Laboratory of Urbanization and Geo-simulation, School of geography and planning, Sun Yat-Sen University, Guangzhou 510275, China

[2] Georges Lemaître Center for Earth and Climate Research (TECLIM), Earth and Life Institute, Université catholique de Louvain, 1348 Louvain-la-Neuve, Belgium

*Correspondence to*: Zhengang Wang (wangzhg33@mail.sysu.edu.cn)

**Abstract.** There is increasing recognition that lateral soil organic carbon (SOC) fluxes due to erosion have imposed an important impact on the global C cycling. Field and experimental studies have been conducted to investigate this topic. It is useful to have a modelling tool that takes into account various soil properties and has flexible resolution and scale options, so that it can be widely used to study relevant processes and evaluate the effect of soil erosion on SOC cycling. This study presents a model that is capable of simulating SOC cycling on a dynamic landscape. It considers all the three C isotopes ($^{12}$C, $^{13}$C and $^{14}$C) with flexible time step and vertical solution of the soil profile. The model gives a 3D representation of soil properties such as $^{137}$Cs activity, SOC stock, and $\delta^{13}$C and $\Delta^{14}$C values. Using the same C cycling processes in stable, eroding and depositional areas, our model is able to reproduce the observed spatial and vertical patterns of C, $\delta^{13}$C values and $\Delta^{14}$C values. This indicates that physical soil redistribution is the main cause of the spatial variability of these C metrics.

## 1 Introduction

There is feedback between the biogeochemistry in the terrestrial system and the radiative forcing. Global warming will result in enhanced soil respiration (Bond-Lamberty et al., 2018) and decreased soil organic carbon (SOC) stock (Knorr et al., 2005). When more SOC is released to the atmosphere, the increased $CO_2$ will enhance the greenhouse effect (Davidson and Janssens, 2006). SOC is the largest organic C pool on the land with approximately 1550 Pg C in the upper meter of soil (Lal, 2008). This is about two times of the C in the atmosphere (ca. 760 Pg C). The annual C flux between soil and the atmosphere is ca. 60 Pg C, which makes the atmosphere $CO_2$ is sensitive to SOC cycling. SOC stock is a balance between input fluxes and output fluxes, which is controlled by various factors such as soil structure, soil parent material, soil pH, climate and land use and management. Climate is an important controlling factor on SOC cycling as it is closely related to the rate of both C input and decomposition (e.g. Davidson and Janssens, 2006;Cox et al., 2000). The terrestrial net primary production and SOC decomposition rate generally decrease with increasing temperature (Koven et al., 2017). Globally, SOC stock decreases with increasing temperature (Jobbágy and Jackson, 2000). Land use is another important factor because different vegetation supplies SOC to the soil with different rates (Mahowald et al., 2017;Maia et al., 2010). The stable isotopic composition of SOC is affected by factors such as vegetation type (C$_3$ vegetation versus C$_4$ vegetation) and Suess effect (Tans et al., 1979). Also, SOC would become enriched in $^{13}$C during the processes of SOC degradation due to preferential mineralization of $^{12}$C (Natelhoffer and Fry, 1988).

Recent studies show that lateral soil redistribution by erosion could also impose an important impact on SOC

stock and soil-atmosphere C exchange (Doetterl et al., 2016;Chappell et al., 2016). During the erosion events, soil aggregates are broken by raindrop and overland flow, which can enhance the SOC decomposition (Van Hemelryck et al., 2011). In the eroding region, SOC in the topsoil is removed by erosion resulting in depletion of SOC. Soil

40    minerals move upwards from below due to soil truncation are added SOC by inputs from plants (Harden et al., 1999). SOC deposited in the depositional settings is buried to depth and well preserved (Van Oost et al., 2012). This lateral redistribution of SOC and the consequent disturbance of SOC cycling of both eroding and depositional regions result in spatial variability in SOC tocks and properties. It was found that eroding sites are depleted of SOC compared to the stable sites while depositional sites are enriched in SOC compared to stable sites in

45    agricultural fields (Li et al., 2007;Van Oost et al., 2005;Yoo et al., 2005). Soil redistribution could lead to difference of SOC stability between eroding and depositional areas. Berhe et al. (2008) found that SOC decomposes faster in the eroding areas compared to depositional areas through signatures of radioactive C isotope. Wang et al. (2014) reported that SOC mineralization rates in the eroding soil profiles are higher than that of depositional soil profiles from results of laboratory soil incubation. Radioactive C isotope gives information on

50    the SOC turnover time, and it is a useful tool to investigate long-term SOC cycling (Trumbore, 2009). SOC redistribution was found to have an effect on SOC radioactive C isotope composition with eroding areas more negative compared to the depositional areas (Berhe et al., 2008).

       Apart from the empirical studies mentioned above, various models have been developed to simulate soil erosion and SOC cycling. At the event scale, there are models simulating processes such as rainfall detachment,

55    sediment entrainment and sediment transport (e.g. Hairsine and Rose, 1992b, a). Some models separate sediments into different sizes, and these models are suitable for simulations the size selectivity in erosion and deposition (Nearing, 1989;Van Oost et al., 2004). These models are further modified to simulate the selectivity of SOC in erosion and deposition (Wilken et al., 2017). Models based on USLE (Universal Soil Loss Equation) utilize annual mean precipitation as model input to simulate the long-term soil erosion (Renard et al., 1997). These models were

60    further added processes of ^{137}Cs deposition, decay and redistribution associated with soil particles, so that they can be calibrated using observed ^{137}Cs data (Van Oost et al., 2003).

       C turnover models have been developed under the condition of stable landscapes (i.e. free of erosion and deposition) to explore the effects of climate, land use and soil environment on SOC cycling. The decomposition of C is often represented by a first-order kinetic rate. Because the SOC is a complex of different components, it is

65    often represented by various pools with respect to C input and decomposition rates in models such as Century (Parton et al., 1987), ICBM (Andren and Katterer, 1997) and RothC (Coleman and Jenkinson, 1995). C fractions obtained in laboratories have been related to C pools in models and used to calibrate model parameters to investigate the turnover of various C pools (Skjemstad et al., 2004;Zimmermann et al., 2007;Wang et al., 2015a). Other SOC properties were also used as constrains to calibrate and validate SOC models. For example, [14]C

70    signatures of SOC has been used to constrain parameters of a multiple-pool SOC model using Bayesian method (Ahrens et al., 2014).

       These multiple-pool C models were further integrated with soil erosion models to make them applicable at eroding landscapes. The balance between the lateral SOC loss by erosion and in situ replacement of lost SOC by photosynthesis at eroding areas was investigated at the profile scale, and they found that proper management is

75    important to maintain the dynamic replacement of lost C (Harden et al., 1999;Billings et al., 2010). At the depositional areas, a profile scale model integrating erosion and SOC cycling processes was calibrated using

observed SOC content and long-term depositional rate, and it was found that sedimentation rate plays an important role in determining burial efficiency of SOC in colluvial settings (Wang et al., 2015b). At the field scale, models that combine SOC redistribution by erosion and SOC dynamics are now well able to reproduce the spatial heterogeneity of SOC stock in fields under land uses with eroding areas depleted of SOC and depositional area enriched in SOC (Van Oost et al., 2005;Rosenbloom et al., 2001;Rosenbloom et al., 2006;Liu et al., 2003;Yoo et al., 2005). However, SOC models that both include C isotopes and are applicable in an eroding landscape are still lacking.

Here, we integrate SOC and soil erosion models and present a model tool that is capable of simulating SOC dynamics in a dynamic landscape. The objectives of this model tool are that (i) it should be a multiple C pool model that is able to represent the complexity of the SOC and to be related to the measurable SOC fractions; (ii) it should include various C isotopes so that it could not only represent these C metrics but also use them to constrain the model; (iii) it should be flexible in terms of spatial and temporal scales so that it would be applicable in various scenarios.

## 2 Methods

Here we present the WATEM_C model that simulates the redistribution of eroded soil and associated C within the catchment and its effects on the dynamics of SOC. The soil redistribution by water erosion is based on the WATEM model (Van Oost et al., 2000) while simulation of C dynamics is based on a three-pool C model (Wang et al., 2015a). All the three C isotopes ($^{12}$C, $^{13}$C and $^{14}$C) are included in our model. Soil advection and diffusion through the soil profile are also included in the model. The model uses flexible time step and vertical resolution of the soil profile so that it can be applied in various settings.

### 2.1 C erosion by water

RUSLE (Revised Universal Soil Loss Equation) (Renard et al., 1997) is used to simulate the long-term potential water erosion ($E_{pot}$; kg m$^{-2}$ yr$^{-1}$):

$$E_{pot} = R * K * L * S * C * P \tag{1}$$

where R is the rainfall erosivity (MJ mm ha$^{-1}$ h$^{-1}$ yr$^{-1}$), K is soil erodibility (kg h MJ$^{-1}$ mm$^{-1}$), L and S are slope steep and length factors, and C and P are factors for the cover management and support practices.

The local erosion rate is considered to equal to the potential erosion rate if the potential erosion rate does not exceed the local transport capacity. The local transport capacity ($T_c$; kg m$^{-1}$ yr$^{-1}$) is calculated as:

$$T_c = k_{tc} * E_{pot} \tag{2}$$

where $k_{tc}$ is the transport capacity coefficient (m).In a grid cell, if its sediment inflow exceeds its local transport capacity, the amount of material transported through the grid equals to the local transport capacity while the remainder is deposited in the grid.

The mobilization of SOC by erosion ($C_{ero}$, kg m$^{-2}$ yr$^{-1}$) is estimated as:

$$C_{ero} = C_{top} * R_{ero} * ER_{ero} \tag{3}$$

where $C_{top}$ is the C content of the top soil layer (%), $R_{ero}$ is the local erosion rate (kg m$^{-2}$ yr$^{-1}$), $ER_{ero}$ is C enrichment ratio in the eroded sediments that equals to the ratio of C content in the eroded sediments to that in the source soils.

The deposited C ($C_{depo}$, kg m$^{-2}$ yr$^{-1}$) can be calculated as:

$$C_{depo} = C_{sed} * R_{depo} * ER_{depo} \tag{4}$$

where $C_{sed}$ is the C content in the transported sediments (%), $R_{depo}$ is the local deposition rate  (kg m$^{-2}$ yr$^{-1}$), $ER_{depo}$ is C enrichment ratio in the deposited sediments that equals to the ratio of the C content in the deposited sediments to that in the bulk transported sediments reaching the depositional sites.

The C enrichment ratios in the mobilized sediments at the erosion sites or in the deposited sediments at the deposited sites are found to be closely related to the local erosion or deposition rates (Wang et al., 2010;Schiettecatte et al., 2008). Thus, the C enrichment ratios of the mobilized and deposited sediments are calculated as:

$$ER_{ero} = a * e^{b*R_{ero}} + 1 \tag{5}$$

$$ER_{depo} = -0.5e^{d*R_{depo}} + 1 \tag{6}$$

where a, b, and d are coefficients.

## 2.2 Soil C turnover

In our model, the three C isotopes ($^{12}$C, $^{13}$C and $^{14}$C) are distinguished. As called in the Century model (Parton et al., 1987), each C isotope is divided into three pools that are referred to as active, slow, and passive pools. The decomposition of these C pools is described using the following differential equations:

$$\frac{d\,^{n}A(z,t)}{dt} = {}^{n}i(z) - {}^{n}k_1 r(z)\,^{n}A(z,t) \tag{7}$$

$$\frac{d\,^{n}S(z,t)}{dt} = h_{AS}\,^{n}k_1 r(z)\,^{n}A(z,t) - {}^{n}k_2 r(z)\,^{n}S(z,t) \tag{8}$$

$$\frac{d\,^{n}P(z,t)}{dt} = h_{AP}\,^{n}k_1 r(z)\,^{n}A(z,t) + h_{SP}\,^{n}k_2 r(z)\,^{n}S(z,t) - {}^{n}k_3 r(z)\,^{n}P(z,t) \tag{9}$$

where $^{n}A(z,t)$, $^{n}S(z,t)$, and $^{n}P(z,t)$ (Mg C ha-1) are the active, slow, and passive pools of C isotope n at depth z (m) and time t (year), respectively; $^{n}i(z)$ (Mg C ha$^{-1}$ yr$^{-1}$) is the input of C isotope n at depth z (m); $h_{AS}$ is the humification coefficients from the active pool to the slow pool, $h_{AP}$ from the active pool to the passive pool, and $h_{SP}$ from the slow pool to the passive pool, respectively; r(z) is a coefficient modifying the variation of C mineralization rate, which denotes the effect of local environmental factors (temperature, humidity, aeration, etc.) at depth z (m); and $^{n}k_1$, $^{n}k_2$, and $^{n}k_3$ (yr$^{-1}$) are the turnover rates at the reference condition (i.e. r(z) = 1) of the active, slow, and passive pools of C isotope n, respectively.

$^{12}$C is preferentially lost through microbial respiration compared to $^{13}$C and $^{14}$C due to its lower atomic weight (Natelhoffer and Fry, 1988). We used discrimination ratio to denote the difference in mineralization between isotopes, and thus the decomposition rate of a $^{13}$C pool ($^{13}$K$_m$, yr$^{-1}$) can be calculated as:

$$^{13}k_m = R_{disc\_13} * {}^{12}k_m \tag{10}$$

where $R_{disc\_13}$ is the discrimination ratio between $^{13}$C and $^{12}$C, $^{12}$k$_m$ is the decomposition rate of the corresponding $^{12}$C pool.

145      Similarly, the decomposition rate of a $^{14}$C pool ($^{14}K_m$, yr$^{-1}$) can be calculated as:

$$^{14}k_m = R_{disc\_14} * {}^{12}k_m \qquad (11)$$

where $R_{disc\_14}$ is the discrimination ratio between $^{14}$C and $^{12}$C.

     r parameter represents the effect of environmental factors affecting C respiration at a given depth, and it is calculated as:

150      $$r(z) = r_0 e^{-r_e z} \qquad (12)$$

where $r_0$ is the value of r parameter at the top soil layer, and $r_e$ (m$^{-1}$) is an exponential decreasing coefficient .

     The input of the C isotopes from plant roots decreases exponentially with depth (Gerwitz and Page, 1974;Van Oost et al., 2005):

$$^{n}i(z) = {}^{n}i_0 e^{-i_e z} \qquad (13)$$

155      where $^{n}i_0$ is the input of C isotope n at the top soil layer (Mg C ha$^{-1}$ yr$^{-1}$); $^{n}i(z)$ (Mg C ha$^{-1}$ yr$^{-1}$) is the input of C isotope n at depth z (m); and $i_e$ (m$^{-1}$) is an exponential decreasing coefficient.

     The $\delta^{13}$C values are expressed in terms of permil (‰) deviation:

$$\delta^{13}C = \left(\frac{(^{13}C/^{12}C)_{Sample}}{(^{13}C/^{12}C)_{PDB}} - 1\right) * 1000 \qquad (14)$$

where $(^{13}C/^{12}C)_{Sample}$ is the abundance ratio of $^{13}$C to $^{12}$C of the soil sample, and $(^{13}C/^{12}C)_{PDB}$ is the ratio of the

160    Pee Dee Belemnite (PDB) as the original standard.

     Thus, the $^{13}$C input can be calculated as:

$$^{13}i = (^{13}C/^{12}C)_{PDB} * \left(1 + \frac{\delta^{13}C(t)}{1000}\right) * {}^{12}i \qquad (15)$$

where $^{13}i$ is the $^{13}$C input (Mg C ha$^{-1}$ yr$^{-1}$) from plant, $^{12}i$ is the $^{12}$C input from plant, $\delta^{13}C(t)$ is $\delta^{13}$C values of C input at time t (yr).

165      We use the atmospheric $\Delta^{14}$C record as a proxy for the isotopic ratio of C input via root and leaf litter input (Hua and Barbetti, 2004). In this paper, the following definition of $\Delta^{14}$C (‰) is used (Stuiver and Polach, 1977):

$$\Delta^{14}C = \left(\frac{(^{14}C/^{12}C)_{Sample}}{A_{ABS}} - 1\right) * 1000 \qquad (16)$$

where $(^{14}C/^{12}C)_{Sample}$ denotes the $^{14}$C:$^{12}$C ratio of the sample, and $A_{ABS}$ denotes the $^{14}$C:$^{12}$C ratio of the standard. $A_{ABS}$ is set to be 1.176 * 10$^{-12}$ (Karlen et al., 1965;Stuiver, 1980).

170      The $^{14}$C input can then be calculated as:

$$^{14}i = A_{ABS} * \left(1 + \frac{\Delta^{14}CO_2^{ATM}(t)}{1000}\right) * {}^{12}i \qquad (17)$$

where $^{14}i$ is $^{14}$C input (Mg C ha$^{-1}$ yr$^{-1}$) from plant, and the $\Delta^{14}CO_2^{ATM}(t)$ is the atmospheric $\Delta^{14}$C signals at time t (yr).

### 2.3 Soil profile evolution due to erosion

175 In the model, soil profiles are represented as a series of soil layers with equal depths. Given that C input and SOC decomposition rate are related with soil depth, SOC cycling is simulated in each layer independently. Because erosion and deposition change the depth of soil profiles, the model updates the depth of soil profiles and the carbon content of each soil layer every time step. At the eroding locations, soils are removed from the top layer and the soil profile is truncated by the amount of eroded soil. At the meantime, SOC is also lost with the local C enrichment

180 ratio. To keep the soil layer with fixed thickness, soils and associated SOC from soil layers below are incorporated into the upper soil layer at the erosion rate. At the depositional locations, because the top layer is buried by the deposited sediments at the deposition rate, soils and associated SOC are moved downward. For all the soil profiles, the component pools of each C isotopes of every layer are updated by homogeneously mixing the component materials every time step.

### 2.4 Advection and diffusion

185 The vertical transport of mineral and organic components of soil is a complex phenomenon driven by a number of distinct mechanisms such as bioturbation (Johnson et al., 2014;Jagercikova et al., 2017), and chemical mobilization (Taylor et al., 2012). We use the advection-diffusion equation to model vertical transport:

$$\frac{dF(z,t)}{dt} = K(z)\frac{d^2}{dz^2}F(z,t) - v(z)\frac{dF(z,t)}{dz} \tag{18}$$

190 where $F(z,t)$ is the concentration of a soil constitute (such as a C isotope pool or ^{137}Cs) at depth z (m) at time t (yr), $v(z)$ (m yr^{-1}) is the advection term at depth z (m) and $K(z)$ (m yr^{-1}) is a diffusion-type mixing coefficient at depth z (m).

K and v are both depth-dependent and are represented using a sigmoidal scaling function:

$$v(z) = \frac{v_0}{1+e^{(v_d*(z-ct))}} \tag{19}$$

195 where $v_d$ (m[-1]) is the depth-attenuation of advection, ct (m) is a constant that is set to 0.15 m, and $v_0$ (m yr^{-1}) is the value of v at the top soil layer.

$$K(z) = \frac{K_0}{1+e^{(K_d*(z-ct))}} \tag{20}$$

where $K_d$ (m[-1]) is the depth-attenuation of diffusion, and $K_0$ (m yr^{-1}) is the value of K at the top soil layer.

### 2.5 ^{137}Cs dynamics

200 ^{137}Cs originates from bomb experiments between 1950 and 1970. It falls to the Earth's surface primarily in association with precipitation and is rapidly adsorbed to soil by clay materials. As the fallout is well constrained, ^{137}Cs has been widely used for tracing the movement of soil and sediment particles in erosion studies (Ritchie and McHenry, 1990). The model reads the values of the local ^{137}Cs fallout. The model then simulates the redistribution of ^{137}Cs by soil erosion and deposition at the land surface associated with soil particles. The model also simulates

205 the downward movement of ^{137}Cs in the soil profile by advection and diffusion. The decay of [137]Cs (half-life of 30.23 year) is also represented in the model.

### 2.6 Model implementation

In order to make the model applicable at various temporal and spatial resolutions, the time step of model iteration and vertical resolution of the soil profile were not fixed, but modifiable as parts of the model input parameters.

210 Given the long-term temporal iteration in SOC cycling processes and the possible large spatial regions where the model may apply, the model was develop using a computation-efficient language (Pascal). The complied executable file can then be called in other environment such as R (R Development Core Team, 2011) where the preparation of the input maps is easier. In our model, the default values of the input parameters were given, and at the same time the user are allowed to assign custom values to the input parameters in the R environment when

215 calling the executable file. The description and relevant parameters regarding SOC cycling are listed in Table 1.

### 2.7 Model application

A set of three scenarios was assumed in order to investigate the effect of advection and diffusion and lateral soil redistribution by erosion on the spatial and vertical distribution of SOC, and $\delta^{13}C$ and $\Delta^{14}C$ values at the landscape scale. Scenario 1: scenario without advection or diffusion or lateral soil redistribution; Scenario 2: scenario with

220 vertical advection and diffusion but without lateral soil redistribution and Scenario 3: scenario with both advection, diffusion and lateral soil redistribution. In order to investigate the effect of plant type change and Suess effect on the $\delta^{13}C$ values of soil profiles, the model was applied in another set of three scenarios. Given that advection and diffusion is comment in soils, we used the scenario with only advection and diffusion as the reference scenario, i.e. Scenario 2 defined above. The other two scenarios are Scenario 4 with plant type change and Scenario 5 with

225 Suess effect.

### 3 Results

### 3.1 $^{137}Cs$

Our simulation shows that, without advection and diffusion, the deposited $^{137}Cs$ is restrained on the surface of soils (Figure 1a). Advection and diffusion transfers soil materials and associated $^{137}Cs$ to the depth, and the amount of

230 transfer is related to the rate of advection and diffusion (Figure 1b). On the eroding landscape, our simulation shows that eroding soil profile is depleted of $^{137}Cs$ compared to the stable soil profile, while the depositional profile is enriched in $^{137}Cs$ in comparison to the stable soil profile (Figure 1c). Also, $^{137}Cs$ in the depositional profile reaches deeper depth compared to the stable soil profile.

### 3.2 SOC

235 Our model is able to reproduce the general pattern of SOC profile of decreasing SOC content with depth in all scenarios despite of rates of advection, diffusion, erosion or deposition (Figure 2). In Scenario 2, higher rates of soil advection and diffusion result in more SOC transferred to the depth, and therefore the difference of SOC content between top layers and bottom layers is smaller under the condition of higher soil advection and diffusion rate compared to SOC profiles of lower advection and diffusion rate (Figure 2b). In Scenario 3, eroding soil profiles

240 contain less SOC compared to the stable soil profiles free of erosion/deposition, while soil profiles at the depositional area are enriched in SOC compare to the stable soil profile (Figure 2c).

### 3.3 $\delta^{13}$C values

In Scenario 1, the $\delta^{13}$C profile shows no variation with depth (Figure 3a). In Scenario 2, the $\delta^{13}$C profile decreases with depth (Figure 3b). The $\delta^{13}$C values of soil profile with higher soil advection and diffusion rates are more negative than that with lower soil advection and diffusion rates (Figure 3b). In Scenario 3, the $\delta^{13}$C values of the eroding profile is less negative than that of the stable soil profile, while soil profiles at the depositional area have more negative $\delta^{13}$C values compared to the stable soil profile (Figure 3c). Our simulation shows that $\delta^{13}$C values increase significantly when the vegetation is converted from $C_3$ vegetation to $C_4$ vegetation (Figure 4). When Suess effect is considered, the $\delta^{13}$C values are lower than that in scenarios that do not consider Suess effect (Figure 4).

### 3.4 $\Delta^{14}$C values

Our model is able to reproduce the general pattern of decreasing $\Delta^{14}$C values with depth in all scenarios despite of rates of soil advection, diffusion, erosion or deposition (Figure 5). In Scenario 2, Soil profiles with higher rates of advection and diffusion have higher $\Delta^{14}$C values compared to profiles with lower vertical transfer rates (Figure 5b). In scenario 3, eroding soil profiles has lower $\Delta^{14}$C values compared to the stable soil profiles, while soil profiles at the depositional area are enriched in $^{14}$C compared to the stable soil profile (Figure 5c).

### 3.5 Spatial variability of soil properties

The model is able to generate a reasonable pattern of soil redistribution with erosion occurring in upland areas and deposition occurring in footslope areas or valleys (Figure 6b). Soil redistribution results in higher $^{137}$Cs inventories in depositional area than eroding area (Figure 6c). The model is also able to generate spatial variability of SOC stock and properties induced by erosion. The depositonal area is enriched in SOC compared with eroding area (Figures 6d and 6e). SOC in the depositional area has lower $\delta^{13}$C values (Figures 6f and 6g) and higher $\Delta^{14}$C values (Figures 6h and 6j) compared to that in the eroding area.

### 4 Discussion

In Scenario 1, the shape of the SOC profile is determined by the vertical patterns of SOC input and decomposition rates, both of which decrease with depth. The fact that the basic shape of the SOC profile can be well represented in Scenario 1 shows that the pattern of C input and decomposition rates is the primary controlling factor on the SOC profile while other factors such as advection and diffusion, erosion or deposition are relatively secondary (Figure 2a). It is natural that higher rates of advection and diffusion would result in more SOC to be transferred to deep layers (Figure 2b). Given that it is less favorable for SOC to be mineralized in deep layers, the transferred SOC by advection and diffusion to the depth would be better preserved. Simulations in Scenario 2 show that SOC stock in the top 1 m under the condition of high advection and diffusion rate (K=0.09, v=0.018) is ca. 14% higher than that under the condition of low advection and diffusion rate (K=0.05, v=0.01). Our model can not only reproduce the vertical pattern of SOC distribution in the soil profile, but that it can also reproduce the spatial variability of SOC stock due to soil redistribution. The simulations under Scenario 3 are consistent with observations that soil erosion results in spatial variability of SOC stock (VandenBygaart et al., 2012;Van Oost et al., 2005;Yoo et al., 2005). This spatial variability was attributed to the replacement of lost at the eroding area and partially preservation of buried SOC in the depositional area (Wang et al., 2015b;Harden et al., 1999;Van Oost et al., 2005).

In Scenario 1, each soil layer is independent from other soil layers, i.e. there is no mass fluxes between soil

280    layers due to the negelation of advection, diffusion and soil redistribution. In this case, each soil layer has its C input and decomposition rates. The $\delta^{13}C$ value of each soil layer is therefore determined by the discrimination ratio between $^{13}C$ and $^{12}C$. If this discrimination ratio is the same between soil layers as implemented in this model, the equilibrium $\delta^{13}C$ profile would be vertically constant (Figure 3a). Due to the fact that the condition of no soil advection and diffusion is not realistic, vertically constant $\delta^{13}C$ profile with depth is rarely reported. When vertical

285    advection and diffusion are considered as in Scenario 2, the transferred SOC from upper layers are isotopically heavier due to degradation compared to the fresh input from plant. This results in an increase of $\delta^{13}C$ values with soil depth (Figure 3b). Our simulation shows that vertical soil advection and diffusion can be one of the main causes of the widely observed increase of $\delta^{13}C$ profiles with depth (Figure 7). At the same depth, soil profile of low soil advection and diffusion rate contains more degraded SOC than profile of high soil advetion and diffusion

290    rate, and therefore soil profile of low soil advection and diffusion rate has less negative $\delta^{13}C$ values. Because erosion and deposition will truncate or bury the original $\delta^{13}C$ profiles, this results in the fact that the eroding soil profile will have higher $\delta^{13}C$ values compared to the stable soil profile while the soil profiles at the depositional sites will have lower $\delta^{13}C$ values in comparision to the stable soil profile (Figure 3c). This is consistent with the observation made in the cropland in Begium (Figure 7). Also, this discrepancy will be more distinct when the

295    erosion or deposition rates become higher. Our simulation shows that soil redistribution by erosion can also cause spatial variability of $\delta^{13}C$ values on an eroding land.

Our model is able to reproduce the widely observed decrease of $\Delta^{14}C$ values with depth in soil profiles (Figure 5). Also, the model can capture the signal of bomb carbon with $\Delta^{14}C$ values at the surface layer being positive. In Scenario 1 with no mass fluxes between soil layers, $\Delta^{14}C$ values is mainly a metrics for the turnover rate or

300    residence time of SOC in each layer. The simulated vertical decrease of $\Delta^{14}C$ values is attributed to the vertical variation of environmental conditions that become less favorable for C mineralization. As discussed for $\delta^{13}C$ profiles, at the same depth soil profile of low soil advection and diffusion rate contains more degraded and old SOC than profile of high soil advetion and diffusion rate, and therefore soil profile of low soil advection and diffusion rate has more negative $\Delta^{14}C$ values (Figure 5b). Similar to $\delta^{13}C$ profiles, erosion and deposition also

305    have a truncation or burial effect of on the $\Delta^{14}C$ profile and this results in the simulation that the eroding soil profiles have more negative $\Delta^{14}C$ values compared to the stable soil profile while the profiles at the depositional sites have less negative $\Delta^{14}C$ values than the stable soil profile (Figure 5c). Our simulation is consistent with the observation from an eroding hillslope in northen California by Berhe et al. (2008) (Figure 8). The causes of more negative $\Delta^{14}C$ values in eroding soil profiles are mainly attributed to the exposure of old SOC from depth, while

310    the observed less negative $\Delta^{14}C$ values in depositional profiles is due to the burial of young SOC from eroding areas.

WATEM_C model focuses on the catchment scale, which allows it to account for processes of both erosion and deposition. It is a spatially distributed model with parcel maps denoting various land use types. Also, it allows accounting for soil conservation measurements, which enables the model to investigate anthropogenic effects (such

315    as land use and management) on erosion and SOC cycling. Compared to previous models, the model presented here is more comprehensive. It includes SOC cycling process and the redistribution of soil and associated SOC by erosion. It is a three-pool C model that discriminates C isotopes ($^{12}C$, $^{13}C$ and $^{14}C$). Thus, it could not only give a three-dimention representation of C, but also C properties such as $\delta^{13}C$ and $\Delta^{14}C$ values (Figure 6). The fact that

our model could reproduce the observed spatial variability of $^{137}$Cs activity, SOC stock, $\delta^{13}$C values and $\Delta^{14}$C
320   values indicates that our model captures the main processes regarding soil redistribution and SOC cycling. The
default values of most of the parameters was set in the executable file generated in Pascal, but they can be assigned
to custom values before running the execable file in R. This allows the model to be applied in various scenarios
by setting relevant parameter values. The model is programmed in a computational efficiency langugag (Pascal),
which makes it suitable to include more C pools and isotopes. Also, the vertical resolution of the soil profile and
325   the temporal resolution of the model iteration is set to be flexible in our model. The users could modify these
parameter based on the requirements of circumstances. The arrange that the model can be called in R makes it
easier to prepare various input maps and to proceed the output of the model.  However, it requires the users to have
experiences in coding in R. The model is designed to simulate only one period with temporally varying inputs on
$^{137}$Cs fallout, $^{13}$C and $^{14}$C input. For the cases of temporal variations such as C input or erosion caused by land use
330   change, the current version of the model is not  able to reprent these processes.

### 5 Conclusions

This paper presents a model (WATEM_C) that is capable of simulating SOC dynamics on an eroding landscape.
It allows tracking the redistribution of soils and associated $^{137}$Cs and SOC within the catchment. The model
captures the soil profile evolution due to erosion and deposition. The SOC dynamics was simulated using a 3 pool
335   C cycling model. All the three C isotopes ($^{12}$C, $^{13}$C and $^{14}$C) are considered in the model and are discriminated
with different cycling rates. The model uses flexible time step and vertical solution of the soil profile. It gives a
3D representation of soil properties such as $^{137}$Cs activity, SOC stock, $\delta^{13}$C values and $\Delta^{14}$C values. The model is
able to reproduce the observed spatial pattern of the SOC stock that eroding soil profiles are depleted of SOC
compared to the stable soil profile while depositional soil profile is enriched of SOC than the stable soil profile.
340   Our simulation is consistent with the observation that the $\delta^{13}$C values of the eroding profile is less negative than
that of the stable soil profile, while soil profiles at the depositional area have more negative $\delta^{13}$C values compared
to the stable soil profile. Our model reproduces the observation that eroding soil profiles has lower $\Delta^{14}$C values
compared to the stable soil profiles, while soil profiles at the depositional area are enriched in $^{14}$C compared to the
stable soil profile. The fact that the spatial patterns of these SOC metrics can be reproduced using the same C
345   cycling processes indicates that physical soil redistribution is the main causes of these spatial variabilities and that
our model captures the most important processes and mechanisms in the SOC cycling on an eroding landscape.
We envisage WATEM_C to be a useful tool in simulating the SOC cycling on an eroding landscape with the wide
cover of various soil properties and flexible choices of resolution options and scenario settings.

*Code availability.* Codes for the model is available at https://github.com/wangzhg33/WATEM_C-version1.0-
350   (last access: 20 September 2019).

*Author contributions.* All the authors were involved in the design of the model. ZW further developed
WATEM_C based on the WATEM model developed by KVO. ZW and KVO wrote the paper together.

355 *Competing interests.* The authors declare that they have no conflict of interest.

*Acknowledgements.* This study was supported by BELSPO (IUAP programme, contract: P7-24) and the
Natural Science Foundation of China (No. 41871014, 41771216, 41501450).

360   Tables

**Table 1. Values of parameters on SOC cycling used this study**

| Parameter | Description | Unit | Values |
|---|---|---|---|
| $^{12}k_1$ | turnover rates of the active $^{12}C$ pool | yr$^{-1}$ | 2.1 |
| $^{12}k_2$ | turnover rates of the active $^{13}C$ pool | yr$^{-1}$ | 0.03 |
| $^{12}k_3$ | turnover rates of the active $^{14}C$ pool | yr$^{-1}$ | 0.002 |
| $h_{AS}$ | humification coefficients from the active pool to the slow pool | - | 0.12 |
| $h_{AP}$ | humification coefficients from the active pool to the passive pool | - | 0.01 |
| $h_{SP}$ | humification coefficients from the slow pool to the passive pool | - | 0.01 |
| $r_0$ | the r parameter at the top soil layer | - | 1 |
| $i_{root}$ | C input from root | Mg C ha$^{-1}$ yr$^{-1}$ | 2.0 |
| $i_{resi}$ | C input from leaf litter | Mg C ha$^{-1}$ yr$^{-1}$ | 0.5 |
| $r_e$ | exponential decreasing coefficient of r with depth | m$^{-1}$ | 3.30 |
| $i_e$ | exponential decreasing coefficient for the root C input with depth | m$^{-1}$ | 20 |
| $R_{disc\_13}$ | discrimination ratio between $^{13}C$ and $^{12}C$ | - | 0.9977 |
| $R_{disc\_14}$ | discrimination ratio between $^{14}C$ and $^{12}C$ | - | 0.996 |

365

Figures
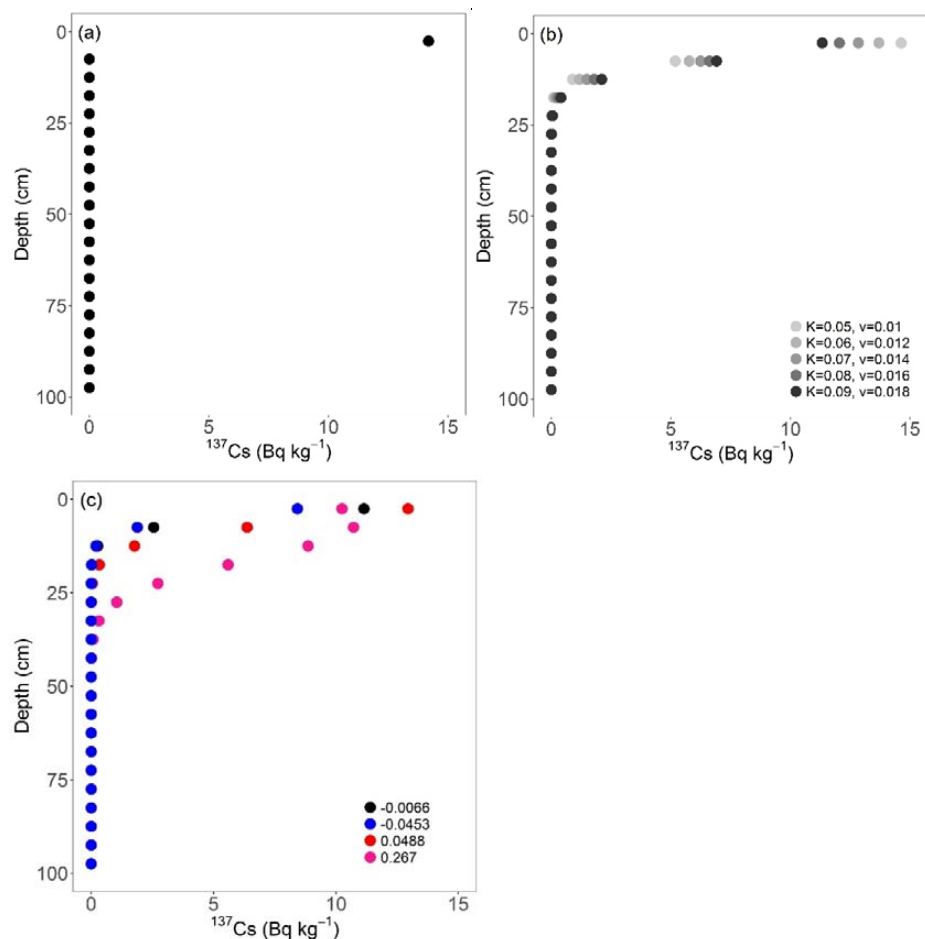
370    **Figure 1: The simulated $^{137}$Cs activity (Bq kg$^{-1}$) profile in (a) Scenario 1, (b) Scenario 2, and (c) Scenario 3. See Section 2.7 for the descriptions of scenarios. In b, K (m$^2$ yr$^{-1}$) is the diffusion coefficient and v (m yr$^{-1}$) is the advection term (Eq. 18). In c, the numbers in the legend are the erosion or deposition rates (cm yr$^{-1}$) with negative values indicating erosion and positive values indicating deposition.**

375
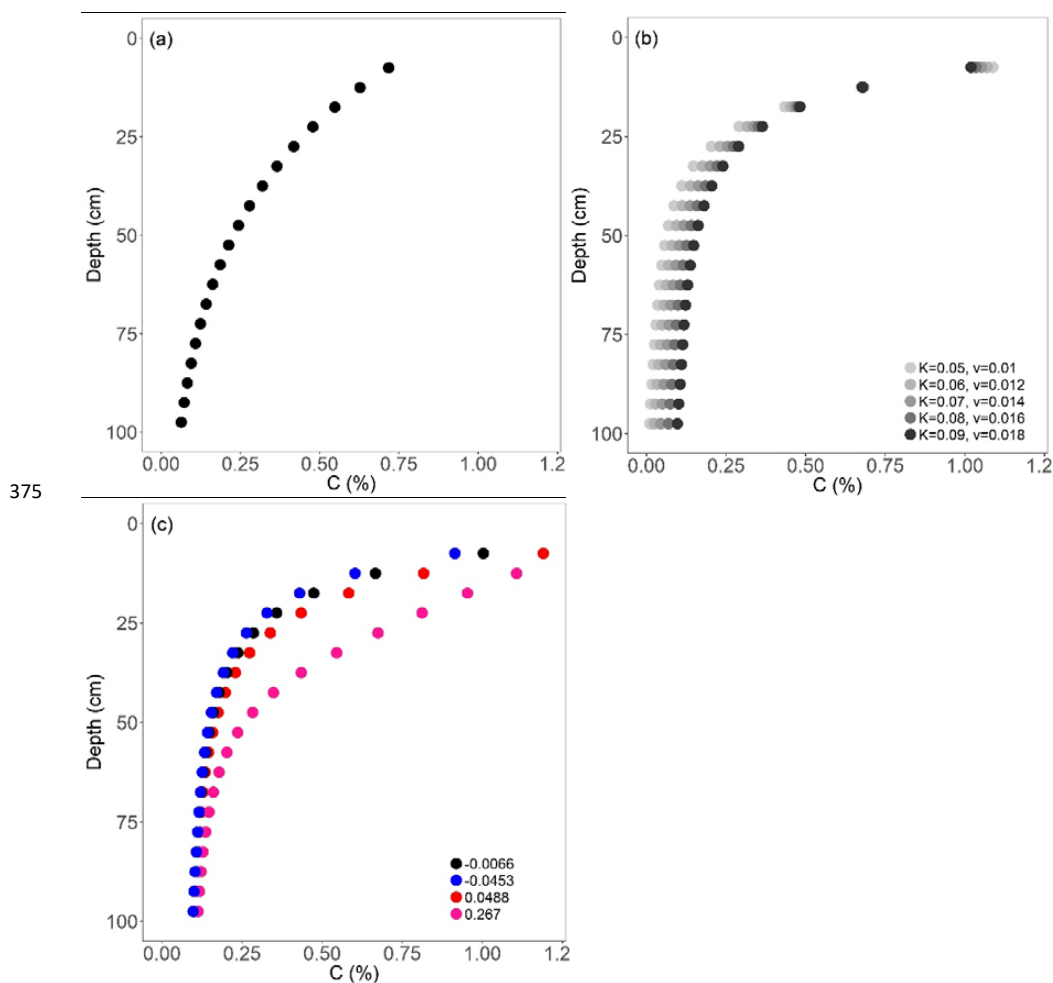
**Figure 2: The simulated C content profiles in (a) Scenario 1, (b) Scenario 2, and (c) Scenario 3. See Section 2.7 for the descriptions of scenarios. In b, K (m² yr⁻¹) is the diffusion coefficient and v (m yr⁻¹) is the advection term (Eq. 18). In c, the numbers in the legend are the erosion or deposition rates (cm yr⁻¹) with negative values indicating erosion and**
380 **positive values indicating deposition.**
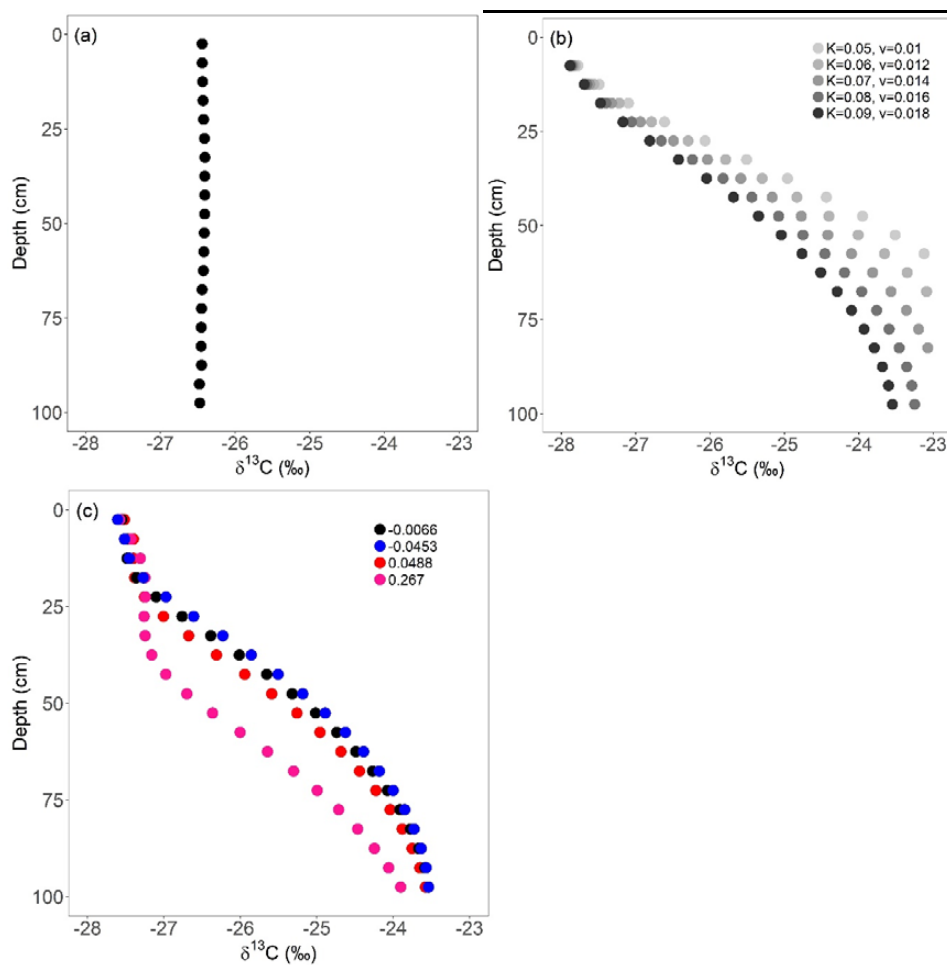
**Figure 3: The simulated δ¹³C profiles in (a) Scenario 1, (b) Scenario 2, and (c) Scenario 3. See Section 2.7 for the**

385    **descriptions of scenarios. In b, K (m² yr⁻¹) is the diffusion coefficient and v (m yr⁻¹) is the advection term (Eq. 18). In**

**c, the numbers in the legend are the erosion or deposition rates (cm yr⁻¹) with negative values indicating erosion and**

**positive values indicating deposition.**

390
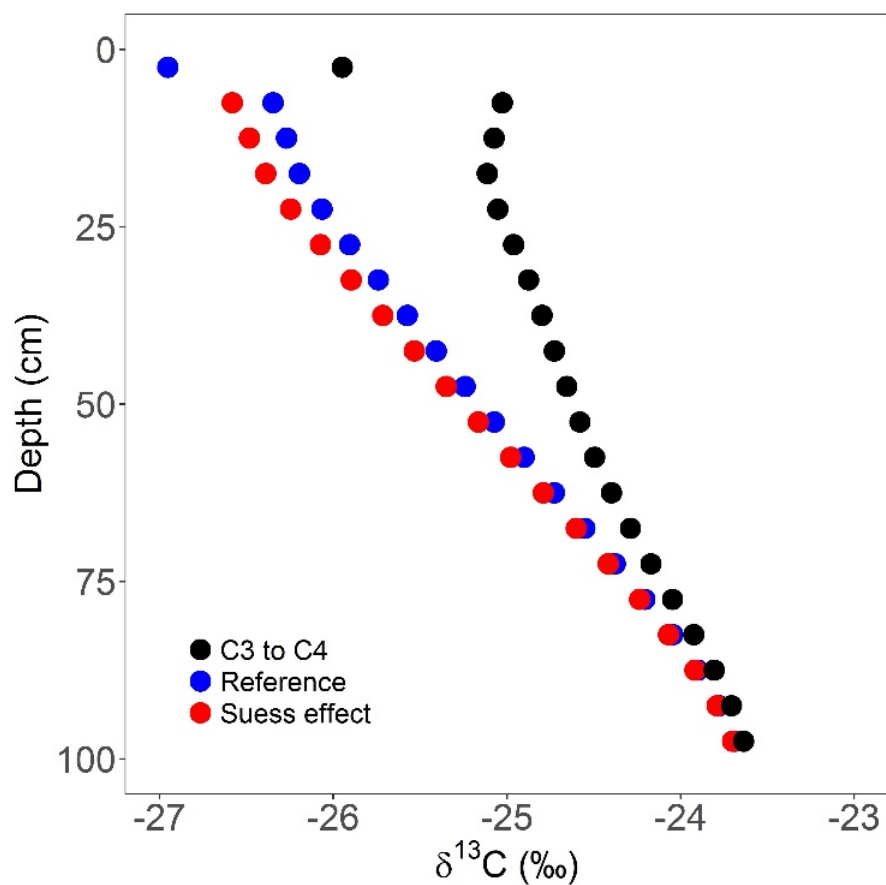
**Figure 4: Effects of plant type change and Suess effect on the δ¹³C profiles.**
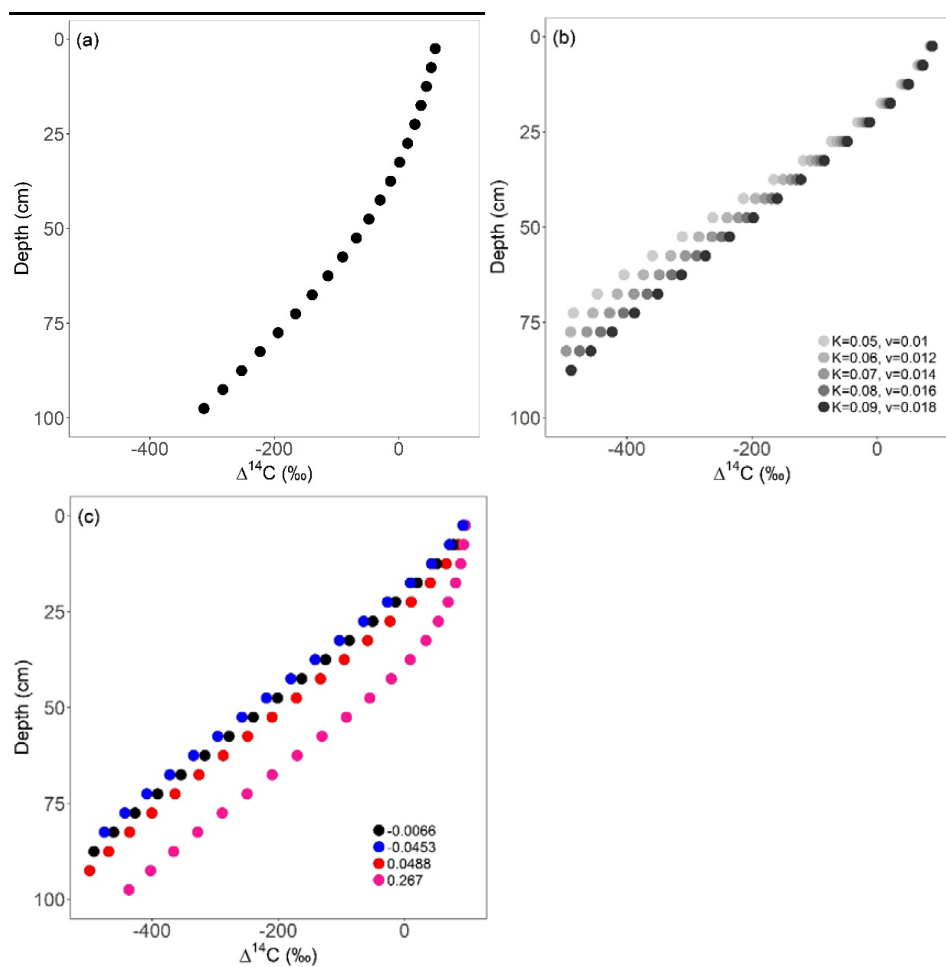
395

**Figure 5: The simulated $\Delta^{14}C$ profiles in (a) Scenario 1, (b) Scenario 2, and (c) Scenario 3. See Section 2.7 for the descriptions of scenarios. In b, K ($m^2$ $yr^{-1}$) is the diffusion coefficient and v ($m$ $yr^{-1}$) is the advection term (Eq. 18). In c, the numbers in the legend are the erosion or deposition rates ($cm$ $yr^{-1}$) with negative values indicating erosion and positive values indicating deposition.**

400

405
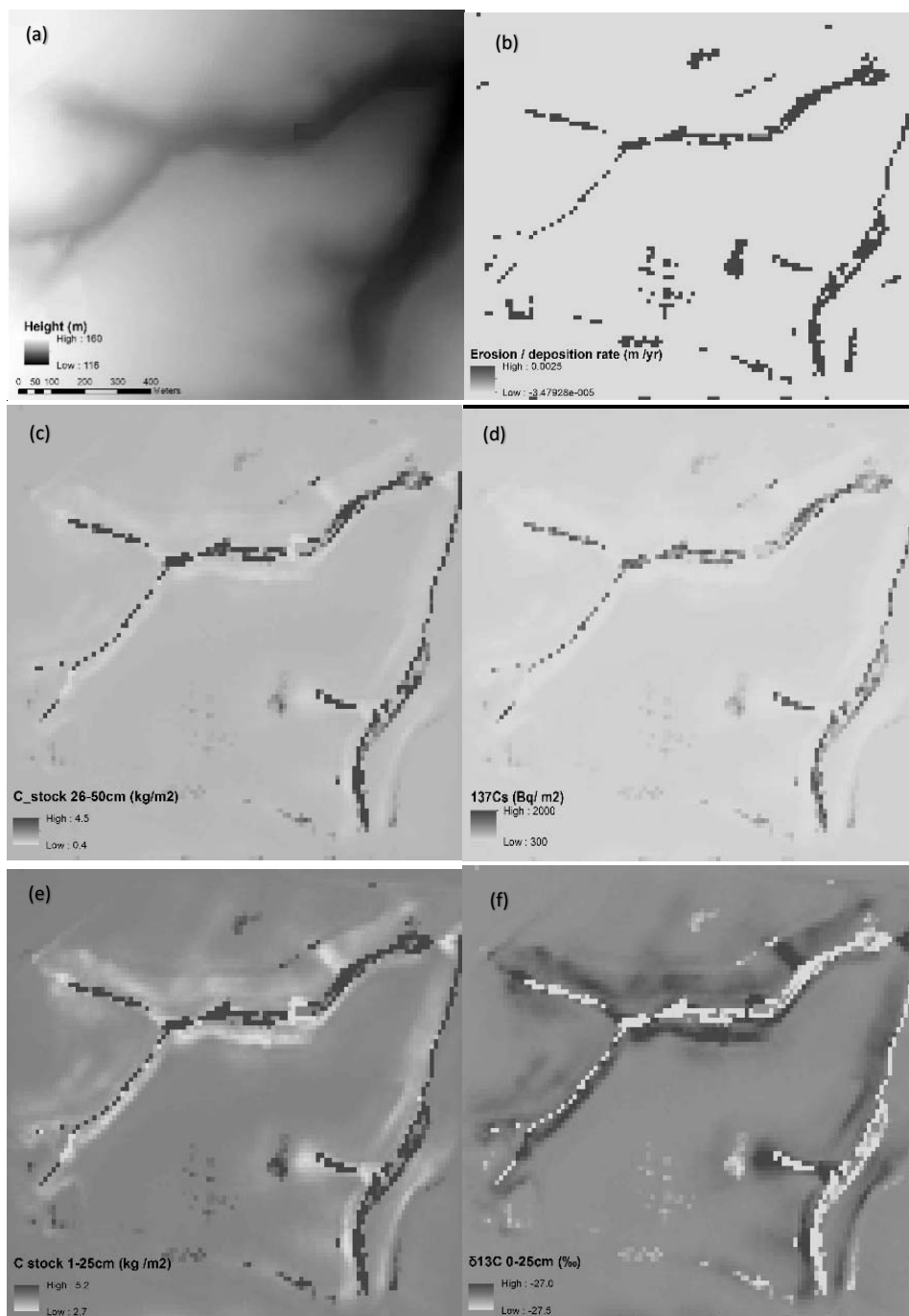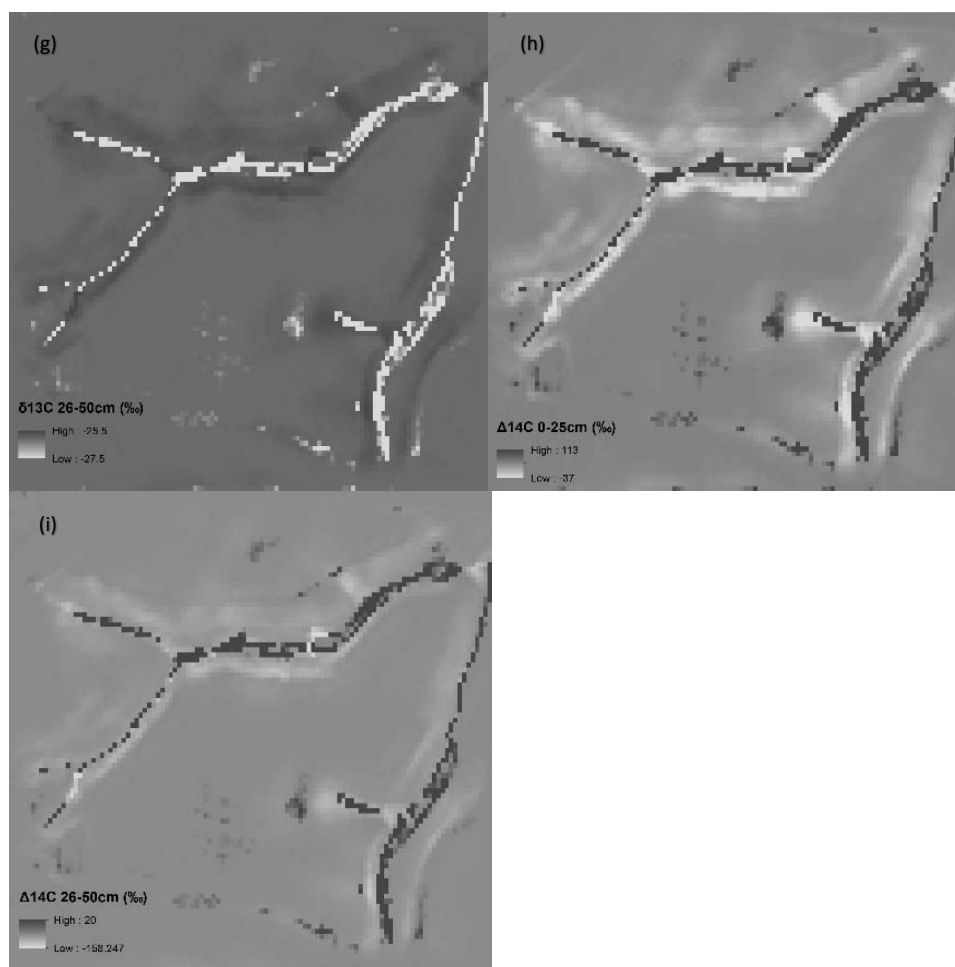
**Figure 6: Model simulations of erosion and erosion-induced spatial variability of SOC stock and isotopic compositions. (a) DEM (digital elevation model) of the field, (b) erosion and deposition rates (positive values indicate deposition and negative values indicate erosion), (c) ^{137}Cs inventory, (d) C stock of topsoil (0-25 cm), (e) C stock of subsoil (26-50 cm), (f) $\delta^{13}$C values of topsoil (0-25 cm), (g) $\delta^{13}$C values of subsoil (26-50 cm), (h) $\Delta^{14}$C values of topsoil (0-25 cm), and (i) $\Delta^{14}$C values of subsoil (26-50 cm).**

410
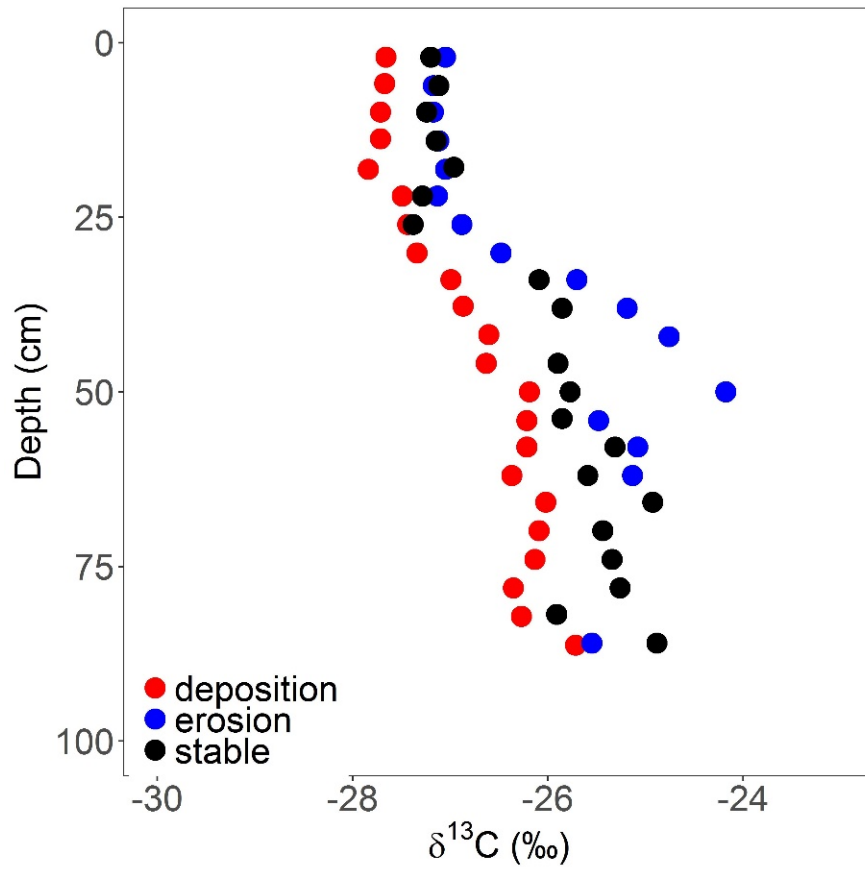
**Figure 7: Observed average δ¹³C profiles of stable, erosion, and depositional areas in a cropland with conventional**
415  **tillage in Hudenburg, Belgium.**
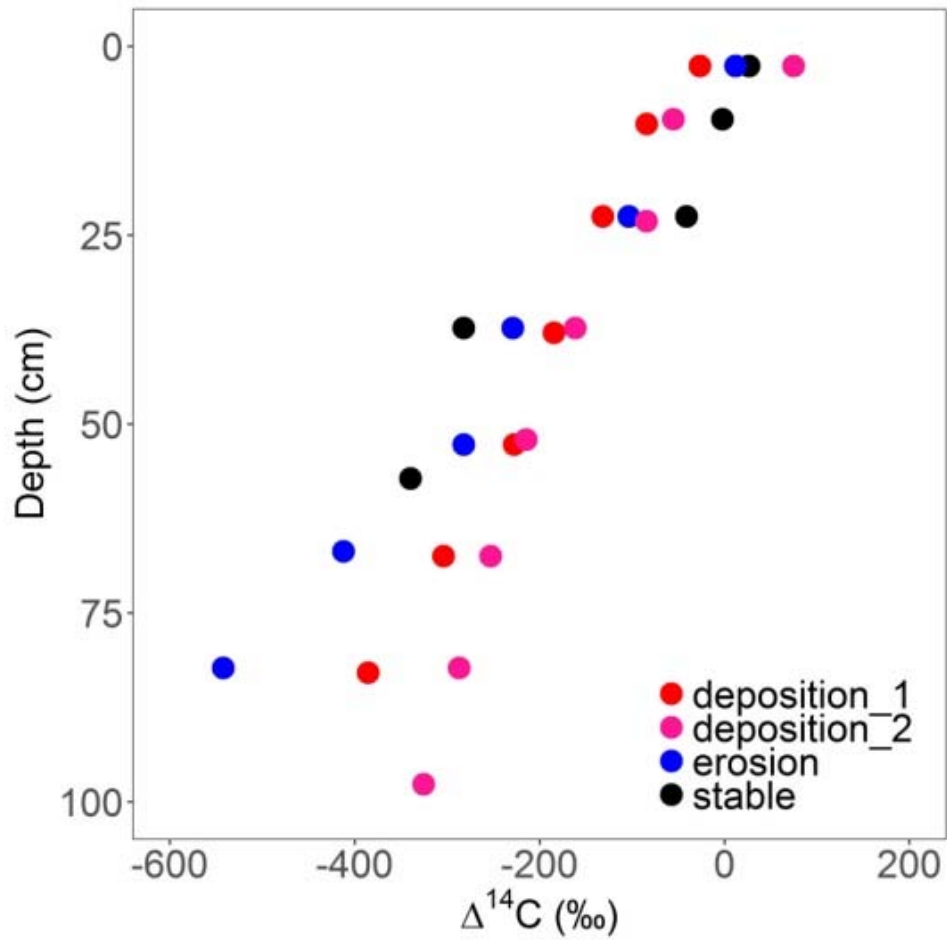
**Figure 8: Observed Δ¹⁴C profiles in an eroding landscape. This figure is adapted from Berhe et al. (2008).**

420

Reference:

Ahrens, B., Reichstein, M., Borken, W., Muhr, J., Trumbore, S. E., and Wutzler, T.: Bayesian calibration of a soil organic carbon model using Δ14C measurements of soil organic carbon and heterotrophic respiration as joint constraints, Biogeosciences, 11, 2147-2168, 10.5194/bg-11-2147-2014, 2014.

425    Andren, O., and Katterer, T.: ICBM: The introductory carbon balance model for exploration of soil carbon balances, Ecological Applications, 7, 1226-1236, 1997.

Berhe, A. A., Harden, J. W., Torn, M. S., and Harte, J.: Linking soil organic matter dynamics and erosion-induced terrestrial carbon sequestration at different landform positions, Journal of Geophysical Research-Biogeosciences, 113, G04039, doi:04010.01029/02008JG000751, doi: 10.1029/2008jg000751, 2008.

430    Billings, S. A., Buddemeier, R. W., Richter, D. D., Van Oost, K., and Bohling, G.: A simple method for estimating the influence of eroding soil profiles on atmospheric $CO_2$, Global Biogeochem. Cycles, 24, doi: 10.1029/2009gb003560, 2010.

Bond-Lamberty, B., Bailey, V. L., Chen, M., Gough, C. M., and Vargas, R.: Globally rising soil heterotrophic respiration over recent decades, Nature, 560, 80-83, 10.1038/s41586-018-0358-x, 2018.

435    Chappell, A., Baldock, J., and Sanderman, J.: The global significance of omitting soil erosion from soil organic carbon cycling schemes, Nature Clim. Change, 6, 187-191, 10.1038/nclimate2829, 2016.

Coleman, K., and Jenkinson, D. S.: ROTHC-26.3 A model for the turnover of carbon in soil: Model description and user guide, Lawes Agricultural Trust, Harpenden, 1995.

Cox, P. M., Betts, R. A., Jones, C. D., Spall, S. A., and Totterdell, I. J.: Acceleration of global warming due to

440    carbon-cycle feedbacks in a coupled climate model, Nature, 408, 184-187, 2000.

Davidson, E. A., and Janssens, I. A.: Temperature sensitivity of soil carbon decomposition and feedbacks to climate change, Nature, 440, 165-173, 2006.

Doetterl, S., Berhe, A. A., Nadeu, E., Wang, Z., Sommer, M., and Fiener, P.: Erosion, deposition and soil carbon: A review of process-level controls, experimental tools and models to address C cycling in dynamic

445    landscapes, Earth-Science Reviews, 154, 102-122, 2016.

Gerwitz, A., and Page, E. R.: An empirical mathematical model to describe plant root systems, Journal of Applied Ecology, 11, 773-781, 1974.

Hairsine, P. B., and Rose, C. W.: Modeling water erosion due to overland flow using physical principles: 2. Rill flow, Water Resour. Res., 28, 245-250, 10.1029/91wr02381, 1992a.

450    Hairsine, P. B., and Rose, C. W.: Modeling water erosion due to overland flow using physical principles: 1. Sheet flow, Water Resour. Res., 28, 237-243, 10.1029/91wr02380, 1992b.

Harden, J. W., Sharpe, J. M., Parton, W. J., Ojima, D. S., Fries, T. L., Huntington, T. G., and Dabney, S. M.: Dynamic replacement and loss of soil carbon on eroding cropland, Global Biogeochem. Cycles, 13, 885-901, 1999.

455    Hua, Q., and Barbetti, M.: Review of tropospheric bomb 14C data for carbon cycle modeling and age calibration purposes, Radiocarbon, 46, 1273–1298, 2004.

Jagercikova, M., Cornu, S., Bourlès, D., Evrard, O., Hatté, C., and Balesdent, J.: Quantification of vertical solid matter transfers in soils during pedogenesis by a multi-tracer approach, Journal of Soils and Sediments, 17, 408-422, 10.1007/s11368-016-1560-9, 2017.

460    Jobbágy, E. G., and Jackson, R. B.: The vertical distribution of soil organic carbon and its relation to climate and vegetation, Ecological Applications, 10, 423-436, 10.1890/1051-0761(2000)010[0423:TVDOSO]2.0.CO;2, 2000.

Johnson, M. O., Mudd, S. M., Pillans, B., Spooner, N. A., Keith Fifield, L., Kirkby, M. J., and Gloor, M.: Quantifying the rate and depth dependence of bioturbation based on optically-stimulated luminescence (OSL)

465    dates and meteoric 10Be, Earth Surface Processes and Landforms, 39, 1188-1196, 10.1002/esp.3520, 2014.

Karlen, I., Olsson, I. U., Kallberg, P., and Kilicci, S.: ABSOLUTE DETERMINATION OF THE ACTIVITY OF TWO C-14 DATING STANDARDS, Arkiv Geofysik., Medium: X; Size: Pages: 465-471, 1965.

Knorr, W., Prentice, I. C., House, J. I., and Holland, E. A.: Long-term sensitivity of soil carbon turnover to warming, Nature, 433, 298-301, Doi 10.1038/Nature03226, 2005.

470    Koven, C. D., Hugelius, G., Lawrence, D. M., and Wieder, W. R.: Higher climatological temperature sensitivity of soil carbon in cold than warm climates, Nature Climate Change, 7, 817, 10.1038/nclimate3421, 2017.

Lal, R.: Carbon sequestration, Philosophical Transactions of the Royal Society B: Biological Sciences, 363, 815-830, 10.1098/rstb.2007.2185, 2008.

Li, Y., Zhang, Q. W., Reicosky, D. C., Lindstrom, M. J., Bai, L. Y., and Li, L.: Changes in soil organic carbon

475    induced by tillage and water erosion on a steep cultivated hillslope in the Chinese Loess Plateau from 1898–1954 and 1954–1998, Journal of Geophysical Research: Biogeosciences, 112, G01021, 10.1029/2005jg000107, 2007.

Liu, S., Bliss, N., Sundquist, E., and Huntington, T. G.: Modeling carbon dynamics in vegetation and soil under the impact of soil erosion and deposition, Global Biogeochem. Cycles, 17, 1074, doi: 10.1029/2002gb002010, 2003.

Mahowald, N. M., Randerson, J. T., Lindsay, K., Munoz, E., Doney, S. C., Lawrence, P., Schlunegger, S., Ward, D. S., Lawrence, D., and Hoffman, F. M.: Interactions between land use change and carbon cycle feedbacks, Global Biogeochemical Cycles, 31, 96-113, 10.1002/2016GB005374, 2017.

Maia, S. M. F., Ogle, S. M., Cerri, C. E. P., and Cerri, C. C.: Soil organic carbon stock change due to land use activity along the agricultural frontier of the southwestern Amazon, Brazil, between 1970 and 2002, Global Change Biology, 16, 2775-2788, 10.1111/j.1365-2486.2009.02105.x, 2010.

Natelhoffer, K. J., and Fry, B.: Controls On Natural Nitrogen-15 And Carbon-13 Abundances In Forest Soil Organic Matter, Soil Sci. Soc. Am. J., 52, 1633-1640, 10.2136/sssaj1988.03615995005200060024x, 1988.

Nearing, M. A.: A process-based soil erosion model for USDA-water erosion prediction project technology, Transactions of the ASAE, v. 32, pp. 1587-1593-1989 v.1532 no.1585, 1989.

Parton, W. J., Schimel, D. S., Cole, C. V., and Ojima, D. S.: Analysis of Factors Controlling Soil Organic Matter Levels in Great Plains Grasslands1, Soil Sci. Soc. Am. J., 51, 1173-1179, 10.2136/sssaj1987.03615995005100050015x, 1987.

R Development Core Team: R: A Language and Environment for Statistical Computing, R Foundation for Statistical Computing, Vienna, Austria3-900051-07-0, 2011.

Renard, K. G., Foster, G. R., Weesies, G. A., McCool, D. K., and Yoder, D. C.: Predicting soil erosion by water: a guide to conservation planning with the Revised Universal Soil Loss Equation (RUSLE). Agriculture Handbook No. 703, USDA-ARS, Washington, DC, 1997.

Ritchie, J. C., and McHenry, J. R.: Application of Radioactive Fallout Cesium-137 for Measuring Soil Erosion and Sediment Accumulation Rates and Patterns: A Review, J. Environ. Qual., 19, 215-233, 10.2134/jeq1990.00472425001900020006x, 1990.

Rosenbloom, N. A., Doney, S. C., and Schimel, D. S.: Geomorphic evolution of soil texture and organic matter in eroding landscapes, Global Biogeochem. Cycles, 15, 365-381, 2001.

Rosenbloom, N. A., Harden, J. W., Neff, J. C., and Schimel, D. S.: Geomorphic control of landscape carbon accumulation, Journal of Geophysical Research-Biogeosciences, 111, G01004, doi: 10.1029/2005jg000077, 2006.

Schiettecatte, W., Gabriels, D., Cornelis, W. M., and Hofman, G.: Enrichment of organic carbon in sediment transport by interrill and rill erosion processes, Soil Sci. Soc. Am. J., 72, 50-55, 2008.

Skjemstad, J. O., Spouncer, L. R., Cowie, B., and Swift, R. S.: Calibration of the Rothamsted organic carbon turnover model (RothC ver. 26.3), using measurable soil organic carbon pools, Soil Research, 42, 79-88, 2004.

Stuiver, M., and Polach, H. A.: Reporting of 14C data – discussion, Radiocarbon, 19, 355–363, 1977.

Stuiver, M.: Workshop on 14C data reporting, Radiocarbon, 22, 964–966, 1980.

Tans, P. P., De Jong, A. F. M., and Mook, W. G.: Natural atmospheric 14C variation and the Suess effect, Nature, 280, 826, 10.1038/280826a0, 1979.

Taylor, A., Blake, W. H., Couldrick, L., and Keith-Roach, M. J.: Sorption behaviour of beryllium-7 and implications for its use as a sediment tracer, Geoderma, 187–188, 16-23, 10.1016/j.geoderma.2012.04.013, 2012.

Trumbore, S.: Radiocarbon and soil carbon dynamics, Annual Review of Earth and Planetary Sciences, 37, 47-66, DOI 10.1146/annurev.earth.36.031207.124300, 2009.

Van Hemelryck, H., Govers, G., Van Oost, K., and Merckx, R.: Evaluating the impact of soil redistribution on the in situ mineralization of soil organic carbon, Earth Surface Processes and Landforms, 36, 427-438, 10.1002/esp.2055, 2011.

Van Oost, K., Govers, G., and Desmet, P.: Evaluating the effects of changes in landscape structure on soil erosion by water and tillage, Landscape Ecology, 15, 577-589, 2000.

Van Oost, K., Govers, G., and Van Muysen, W.: A process-based conversion model for caesium-137 derived erosion rates on agricultural land: An integrated spatial approach, Earth Surface Processes and Landforms, 28, 187-207, 2003.

Van Oost, K., Beuselinck, L., Hairsine, P. B., and Govers, G.: Spatial evaluation of a multi-class sediment transport and deposition model, Earth Surface Processes and Landforms, 29, 1027-1044, 2004.

Van Oost, K., Govers, G., Quine, T. A., Heckrath, G., Olesen, J. E., De Gryze, S., and Merckx, R.: Landscape-scale modeling of carbon cycling under the impact of soil redistribution: The role of tillage erosion, Global Biogeochem. Cycles, 19, 10.1029/2005gb002471, 2005.

Van Oost, K., Verstraeten, G., Doetterl, S., Notebaert, B., Wiaux, F., Broothaerts, N., and Six, J.: Legacy of human-induced C erosion and burial on soil–atmosphere C exchange, Proceedings of the National Academy of Sciences, 109, 19492-19497, doi: 10.1073/pnas.1211162109, 2012.

VandenBygaart, A. J., Kroetsch, D., Gregorich, E. G., and Lobb, D.: Soil C erosion and burial in cropland, Global Change Biology, 18, 1441-1452, doi: 10.1111/j.1365-2486.2011.02604.x, 2012.

Wang, Z., Govers, G., Steegen, A., Clymans, W., Van den Putte, A., Langhans, C., Merckx, R., and Van Oost, K.: Catchment-scale carbon redistribution and delivery by water erosion in an intensively cultivated area, Geomorphology, 124, 65-74, 2010.

540 Wang, Z., Van Oost, K., Lang, A., Quine, T., Clymans, W., Merckx, R., Notebaert, B., and Govers, G.: The fate of buried organic carbon in colluvial soils: a long-term perspective, Biogeosciences, 11, 873-883, 10.5194/bg-11-873-2014, 2014.

Wang, Z., Doetterl, S., Vanclooster, M., van Wesemael, B., and Van Oost, K.: Constraining a coupled erosion and soil organic carbon model using hillslope-scale patterns of carbon stocks and pool composition, Journal of 545 Geophysical Research: Biogeosciences, 2014JG002768, 10.1002/2014JG002768, 2015a.

Wang, Z., Van Oost, K., and Govers, G.: Predicting the long-term fate of buried organic carbon in colluvial soils, Global Biogeochemical Cycles, 29, 65-79, 10.1002/2014GB004912, 2015b.

Wilken, F., Fiener, P., and Van Oost, K.: Modelling a century of soil redistribution processes and carbon delivery from small watersheds using a multi-class sediment transport model, Earth Surf. Dynam., 5, 113-124, 550 10.5194/esurf-5-113-2017, 2017.

Yoo, K., Amundson, R., Heimsath, A. M., and Dietrich, W. E.: Erosion of upland hillslope soil organic carbon: Coupling field measurements with a sediment transport model, Global Biogeochem. Cycles, 19, Gb3003, 10.1029/2004gb002271, 2005.

Zimmermann, M., Leifeld, J., Schmidt, M. W. I., Smith, P., and Fuhrer, J.: Measured soil organic matter 555 fractions can be related to pools in the RothC model, European Journal of Soil Science, 58, 658-667, 10.1111/j.1365-2389.2006.00855.x, 2007.